Electrochimica Acta 56 (2011) 4518–4525

Contents lists available at ScienceDirect

Electrochimica Acta

journal homepage: www.elsevier.com/locate/electacta

Role of the diffuse layer in acidic and alkaline fuel cells

Isaac Sprague, Prashanta Dutta*

School of Mechanical and Materials Engineering, Washington State University, Pullman, WA 99164-2920, USA

ARTICLE INFO

Article history:
Received 17 December 2010
Received in revised form 13 February 2011
Accepted 15 February 2011
Available online 23 February 2011

Keywords:
Alkaline fuel cell
Acidic electrolyte
Alkaline electrolyte
Electric double layer
Laminar flow fuel cell

ABSTRACT

A numerical model is developed to study electrolyte dependent kinetics in fuel cells. The model is based on the Poisson–Nernst–Planck (PNP) and generalized-Frumkin–Butler–Volmer (gFBV) equations, and is used to understand how the diffuse layer and ionic transport play a role in the performance difference between acidic and alkaline systems. The laminar flow fuel cell (LFFC) is used as the model fuel cell architecture to allow for the appropriate comparison of equivalent acidic and alkaline systems. We study the overall cell performance and individual electrode polarizations of acidic and alkaline fuel cells for both balanced and unbalanced electrode kinetics as well as in the presence of transport limitations. The results predict cell behavior based on electrolyte composition that strongly correlates with observed experimental results from literature and provides insight into the fundamental cause of these results. *Specifically, it is found that the working ion concentration at the reaction plane plays a significant role in fuel cell performance including activation losses and the response to different kinetic rates at an individual electrode*. The working ion and the electrode where its consumed are different for acidic and alkaline fuel cells. Therefore, we compare the role of the diffuse region in both acidic and alkaline fuel cells. *From this we conclude that oxidant reduction at the cathode and slow fuel oxidation (such as alcohol oxidation) can be improved with an alkaline electrolyte*.

1. Introduction

The basic principle of fuel cell technology has been known since the late 1830s but it was not until the mid twentieth century that it was proven to be a viable option for power generation with the introduction of the alkaline fuel cell. During that time, alkaline fuel cells were the prevalent fuel cell technology and as such were given substantial research interest. The most common alkaline fuel cell is the mobile electrolyte fuel cell whose basic physical structure consists of an anode and a cathode separated by a flowing alkaline electrolyte solution [1]. However, despite several advantages over their acidic counter parts, including superior oxidant reduction and alcohol oxidation, alkaline fuel cells suffer some major limitations at the device level that lead to significant reduction in interest in alkaline fuel cells [2].

In recent years, acidic fuel cells (i.e. proton exchange membrane fuel cells (PEMFC)) have risen to prominence in the fuel cell community as the preferred low temperature solution. The PEMFC uses a solid acidic membrane to separate the anode and cathode [1] and has been studied extensively both experimentally and numerically [3–6]. There have also been mathematical models presented in literature for alkaline fuel cells [7–13] although they are significantly less abundant. These models tend to focus on the system level description of fuel cells (especially for alkaline fuel cells), and to our knowledge there are no theoretical works for comparing fundamental differences in acidic and alkaline fuel cells.

At the basal level, the primary differences between and acidic and alkaline fuel cell are the electrolyte and the working ion. Here we are using "working ion" to mean the ion that is produced at one electrode and migrates across the electrolyte to be consumed at the other electrode, thus completing the circuit. To study how the electrolyte and working ion affect fuel cell operation, the ionic transport within the electrolyte must be modeled explicitly. Additionally, it is essential to include electric double layer (EDL) effects due to the strong influence the diffuse layer has on ionic concentrations at the reaction plane of an electrode [14]. These phenomena can be modeled using the Poisson–Nernst–Planck (PNP) equations. The PNP equations have successfully been applied to galvanic cells [15,16] and fuel cells [17–20] in the literature.

At the functional level one of the primary differences between acidic and alkaline fuel cells is that oxygen reduction and simple alcohol oxidation kinetics are superior in alkaline fuel cells than in acidic fuel cells [2]. The fundamental cause of the improved kinetics in alkaline cells is of paramount interest [21–24]. One general explanation was offered by Spendlow and Wieckowski [21], who suggested that the working potential range of an electrochemical process is often limited to a range in which water is stable. This range shifts with increasing pH according to the Nernst equation, which can affect the local double layer structure at the electrode thus impacting the kinetics. However, despite all the research there

* Corresponding author. Tel.: +1 509 335 7989; fax: +1 509 335 4662.
E-mail address: dutta@mail.wsu.edu (P. Dutta).

0013-4686/$ – see front matter © 2011 Elsevier Ltd. All rights reserved.
doi:10.1016/j.electacta.2011.02.060

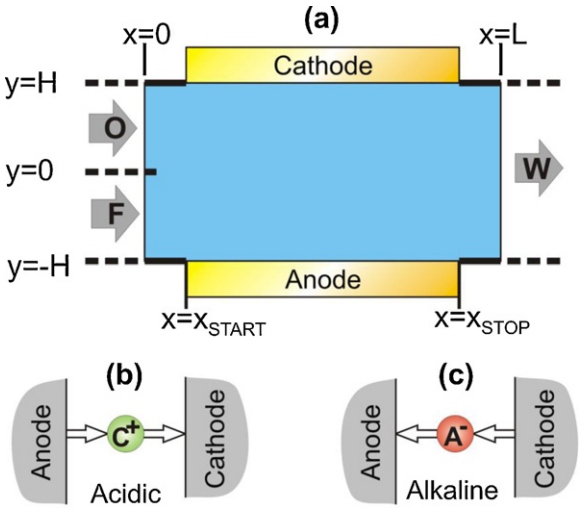

Fig. 1. (a) Schematic of the computational domain for a LFFC depicting two inlets (fuel and oxidant) and a single outlet (waste). The walls are located at $Y = \pm H$ with the electrodes in the domain $x_{Start} \le x \le x_{Stop}$. The working ion type and flux direction within the electrolyte are depicted for both (b) acidic and (c) alkaline media. In the case of an acidic fuel cell, cations (C^+) migrate from the anode to the cathode while in an alkaline fuel cell, anions (A^-) migrate from the cathode to the anode.

does not seem to be an axiomatic justification for the altered electrode kinetics between acidic and alkaline media. *In this work we offer a unique explanation of altered electrode kinetics by studying how the diffuse layer and ionic transport play a significant role in the performance differences of acidic and alkaline systems.*

For direct comparison between acidic and alkaline fuel cells, a fuel cell architecture that is compatible with both acidic and alkaline fuel cells must be selected to isolate the electrolyte and ionic transport effects from the physical system differences. One such architecture is the laminar flow fuel cell (LFFC) which has been studied in acidic [25–27] and alkaline [28,29] media due to their excellent fuel and electrolyte flexibility. Another benefit of selecting a LFFC for our comparison is their relatively simplistic design and operation, which is ideal for mathematical analysis. Several models of LFFCs have been presented in the literature [30–34].

In our previous works we presented a mathematical model for a LFFC based on the PNP equations for ionic transport and a generalized Frumkin–Butler–Volmer (gFBV) equation for electrode kinetics [19,20]. The focus of this work is to study a LFFC using the gFBV-PNP model adapted for acidic and alkaline media. We studied overall device performance, the anode and cathode polarizations for each case, and the performance response to changing reaction kinetics as well as reactant concentrations in both acidic and alkaline fuel cells.

2. Model development

Fig. 1a shows the schematic of the laminar flow fuel cell system with separate fuel and oxidant inlets and a single waste outlet. For simplicity, the computational domain is selected from just upstream of the electrodes at $x = 0$ to just downstream of the electrodes at $x = L$. The channel walls are located at $y = \pm H$ with the anode defined at $y = -H$ and the cathode at $y = H$. The anode and cathode electrodes are located between $x = x_{Start}$ and $x = x_{Stop}$ where $0 < x_{Start} < x_{Stop} < L$. A simple redox reaction of fuel (F) and oxidant (O) producing waste (W) is considered for both the acidic and alkaline systems. The overall stoichiometric equation is:

$$S_F \cdot F + S_O \cdot O \rightarrow S_{W,F} \cdot W_F + S_{W,O} \cdot W_O \quad (1)$$

where W_F is the waste produced by fuel oxidation and W_O is the waste produced by oxidant reduction. These terms may be neglected if there is no waste (e.g. hydrogen oxidation) or if the waste is water which is adsorbed into an aqueous solution at a constant chemical potential (as is the case for oxygen reduction). For methanol oxidation, however, the waste W_F is CO_2 which is a gas but present in concentrations far below its solubility limit and remains dissolved in the aqueous bulk electrolyte.

For ease of analysis, the reaction is considered to proceed in the presence of a simple binary electrolyte consisting of an anion (A^-) and a cation (C^+) each of unit charge, $z_c = -z_A = 1$. The working ion and half reactions of fuel oxidation and oxidant reduction depend on the type of system considered, acidic or alkaline. For an acidic electrolyte the cation is the working ion, being produced at the anode and consumed at the cathode, Fig. 1b. Therefore, in the acidic case the half reactions become:

$$S_F \cdot F \rightarrow S_C \cdot C^+ + n \cdot e^- + S_{W,F} \cdot W_F \quad (2a)$$

$$S_C \cdot C^+ + n \cdot e^- + S_O \cdot O \rightarrow S_{W,O} \cdot W_O \quad (2b)$$

where n is the number of electrons involved in the reaction and depends on the specific reactants in the overall reaction. On the other hand, for an alkaline electrolyte the anion is the working ion which is produced at the cathode and consumed by the anode, Fig. 1c. Therefore, the half reactions for the alkaline case become:

$$S_F \cdot F + S_A \cdot A^- \rightarrow n \cdot e^- + S_{W,F} \cdot W_F \quad (3a)$$

$$S_O \cdot O + n \cdot e^- \rightarrow S_A \cdot A^- + S_{W,O} \cdot W_O \quad (3b)$$

It is assumed that in an acidic fuel cell the anion is inert, while in an alkaline fuel cell the cation is the inert ion.

2.1. Electrode kinetics

The rate at which the above half reactions proceed is determined by the electrode kinetics at the electrolyte–electrode interface located at the anode and cathode in the presence of the EDL. The electrode kinetics are governed by the generalized Frumkin–Butler–Volmer equation (gFBV), which gives the net current for a specific half reaction as a function of the potential drop across the inner region of the EDL and the concentration of the reactants at interface (reaction plane) of the inner and outer regions. The Stern model of the electric double layer assumes a linear potential drop across the inner region, called the Stern layer, that is continuous with the potential in the outer region, called the diffuse layer [35]. The gFBV equations for the fuel and oxidant reactions in an acidic fuel cell are respectively:

$$J_{F,Net} = J_{F,O} - J_{F,R} = Fn[(K_{F,O}^{Acidic} C_F e^{((1-\beta)\Delta\phi_S F)/RT}) - (K_{F,R}^{Acidic} C_{C^+} C_W e^{-(\beta\Delta\phi_S F)/RT})] \quad (4a)$$

$$J_{O,Net} = J_{O,O} - J_{O,R} = Fn[(K_{O,O}^{Acidic} C_W e^{((1-\beta)\Delta\phi_S F)/RT}) - (K_{O,R}^{Acidic} C_O C_{C^+} e^{-(\beta\Delta\phi_S F)/RT})] \quad (4b)$$

where $\Delta\phi_S$ is the potential difference across the Stern layer. From this equation it is clear that the net current from a specific half reaction is the difference between the oxidation (forward) and reduction (reverse) currents. Similarly, the gFBV equations for the fuel and oxidant reactions in an alkaline fuel cell are respectively:

$$J_{F,Net} = J_{F,O} - J_{F,R} = Fn[(K_{F,O}^{Alkaline} C_F C_{A^-} e^{((1-\beta)\Delta\phi_S F)/RT}) - (K_{F,R}^{Alkaline} C_W e^{-(\beta\Delta\phi_S F)/RT})] \quad (5a)$$

$$J_{O,Net} = J_{O,O} - J_{O,R} = Fn[(K_{O,O}^{Alkaline} C_W C_{A^-} e^{((1-\beta)\Delta\phi_S F)/RT}) - (K_{O,R}^{Alkaline} C_O e^{-(\beta\Delta\phi_S F)/RT})] \quad (5b)$$

Table 1
Relationships between nondimensional and dimensional rate constants in acidic and alkaline media. Here $\alpha = 1/C_W^{Bulk}$..

Acidic fuel cell	Alkaline fuel cell
$K_{F,O}^{Acidic} = \hat{K}_{F,O}(D_C/2H)$	$K_{F,O}^{Alkaline} = \hat{K}_{F,O}(D_A/2H\,C_E^{Bulk})$
$K_{F,O}^{Acidic} = \hat{K}_{F,R}(\alpha D_C/2H)$	$K_{F,R}^{Alkaline} = \hat{K}_{F,R}(\alpha D_A C_E^{Bulk}/2H)$
$K_{O,O}^{Acidic} = \hat{K}_{O,O}(\alpha D_C C_E^{Bulk}/2H)$	$K_{O,O}^{Alkaline} = \hat{K}_{O,O}(\alpha D_A/2H)$
$K_{O,R}^{Acidic} = \hat{K}_{O,R}(D_C/2H\,C_E^{Bulk})$	$K_{O,R}^{Alkaline} = \hat{K}_{O,R}(D_A/2H)$

The half reactions are allowed to proceed at both the anode and cathode, and the net current for a specific electrode is the sum of the fuel and oxidant reaction currents:

$$J_{Net,El} = J_{F,Net} + J_{O,Net} \tag{6}$$

where $J_{F,Net}$ is a positive quantity and $J_{O,Net}$ is a negative quantity. The magnitudes of $J_{F,Net}$ and $J_{O,Net}$ are determined by the reactants present at the electrode of interest and the sign of the potential difference across the Stern layer.

2.2. Dimensionless rate constants

Closer inspection of Eqs. (4)–(6) reveals that each component of the net electrode current has different concentration dependencies. A result of this is that for a given set of rate constants the magnitude of the net current will be different for acidic and alkaline kinetics. Therefore, to achieve an equivalent comparison between the two systems, the rate constants are specified in dimensionless form. The dimensional current is presented as $J_{Net} = \hat{J}_{Net}(D_E FnC_E^{Bulk}/2H)$ where $\hat{J}_{Net}$ is the nondimensional current. From this scaling, it is straightforward to determine the scale factors for each rate constant in Eqs. (4) and (5). Table 1 provides a summary of the dimensional and nondimensional relationships for each rate constant.

2.3. Governing equations

The mathematical model used for the present analysis is based on the PNP equations and has been presented elsewhere [19,20]. In brief, the net flux density of a specific species is the sum of the advection, diffusion, and electromigration flux densities and is given by:

$$N_i = \vec{V}C_i - D_i\nabla C_i - z_i\omega_i FC_i\nabla\phi \tag{7}$$

where i indicates the species considered and $i = C^+$, A^-, F, O, W_F, W_O. The concentration distributions are assumed steady and the Nernst–Planck equation for each species can be written as:

$$\nabla \cdot N_i = 0 \tag{8}$$

It is clear that the concentration distribution of an ion is coupled to the electrolyte potential through the migration flux. The potential distribution within the electrolyte is governed by the electrostatic Poisson equation:

$$-\nabla\cdot(\varepsilon_E\nabla\phi) = \rho_e = F\sum z_iC_i \tag{9}$$

where ρ_e is the charge density. The bulk flow in the microchannel is governed by the steady-state Navier–Stokes and continuity equations:

$$\nabla\cdot(\rho\vec{V}\vec{V}) = \nabla\cdot(\mu\nabla\vec{V}) - \nabla P - \rho_e(\nabla\phi) \tag{10a}$$

$$\nabla\cdot(\rho\vec{V}) = 0 \tag{10b}$$

The flow is coupled to the charge density and potential gradient in the electrolyte as evidenced by the last term on the right hand side of Eq. (10a). This term has been shown to be small and can be neglected without affecting the results for fuel cell performance [20].

2.4. Boundary conditions

The computational domain depicted in Fig. 1a has five basic boundaries: the fuel inlet, oxidant inlet, outlet, walls, and electrodes. Fuel and oxidant are specified as their bulk concentrations at their respective inlets and zero at the other inlet. The ionic concentrations are specified as their bulk concentrations at both inlets. Electrode kinetics are applied as boundary conditions for Eq. (8) at the electrodes by relating the flux density to the net electrode current. Finally, an adaptation of the Stern model is used as a mixed (Robin) boundary condition for electrolyte potential at reaction plane, $\phi_{RP} = \psi_{El} + (\varepsilon_S/C_S)(\partial\phi/\partial Y)$. This also gives the potential difference across the Stern layer $\Delta\phi_S = \psi_{El} - \phi_{RP}$ which is used in the electrode kinetics (Eqs. (4) and (5)).

2.5. Numerical formulation

The mathematical system presented above is highly nonlinear and strongly coupled. This system is further complicated by the nonlinear boundary conditions necessary for electrode kinetics. An in-house numerical tool was developed to solve this system for a LFFC in the 2-dimensional domain presented in Fig. 1a and is capable of resolving the full PNP model in the microscopic region of the electrolyte–electrode interface. The details of this numerical model are presented elsewhere [20]. The numerical results were performed with an Intel Core i7-975 3.33 GHz processor operating 4 cores. Solution times depend on the problem inputs (e.g. transport limited results take longer to converge) and range from 1 to 5 h.

3. Results and discussion

The physical structure of the LFFC considered for both the acidic and alkaline fuel cells is presented in Fig. 1a. The half channel height was set to $H = 0.5$ mm and the channel length was set to $L = 5$ mm. The electrode dimensions were $x_{Start} = 0.5$ mm and $x_{Stop} = 4.5$ mm. The stoichiometric coefficients for the neutral species were $S_F = S_O = S_{W,F} = S_{W,O} = 1$ and for the cation and anion they were $S_C = S_A = 6$. The number of electrons involved in the reaction, n, was also set to 6. The nominal bulk concentrations at the inlets were specified as $C_F^{Bulk} = C_O^{Bulk} = C_E^{Bulk} = 100$ mM and the nominal concentration of waste in the bulk solution was set to a negligible quantity. The bulk flow is assumed to be fully developed in each inlet and therefore a parabolic profile was specified at each inlet with a maximum velocity of 1 mm s^{-1}. The remaining parameters are identical to that in Ref. [19].

To analyze the full operating range of the LFFC from short circuit to open circuit, the cathode potential (ψ_{Ca}) was varied while the anode potentail (ψ_{An}) was held constant. The cathode potential ranged form zero to $\psi_{Ca} = \psi_{OCP}$ where the open circuit potential was determined by when the total cathode current density, $J_{Cell,Ca}$, is zero. The total electrode current density can be calculated by:

$$J_{Cell,El} = \frac{1}{(x_{End} - x_{Start})}\int_{x_{Start}}^{x_{End}} J_{Net,El}(x)dx \tag{11}$$

and the overall current density for the device is then $J_{Cell} = J_{Cell,An} = -J_{Cell,Ca}$.

3.1. Cell performance with balanced kinetics

The overall cell performance and electrode polarizations are presented in Fig. 2 for an acidic (a) and alkaline (b) fuel cell with

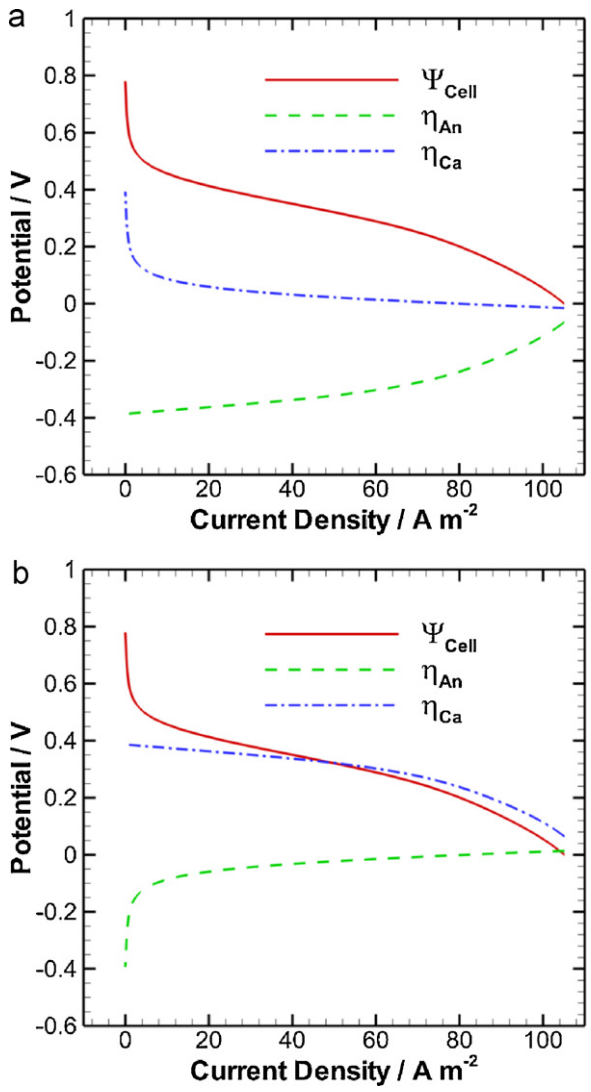

Fig. 2. Overall VI and electrode polarizations for a LFFC using an (a) acidic electrolyte and an (b) alkaline electrolyte. The electrode polarizations are presented by showing the individual electrode overpotentials as a function of cell current density. The (normalized) rate constants are $\hat{K}_{F,O} = \hat{K}_{O,R} = 1$ and $\hat{K}_{F,R} = \hat{K}_{O,O} = 1 \times 10^{-6}$; the concentrations in the bulk electrolyte are $C_F^{Bulk} = C_O^{Bulk} = C_E^{Bulk} = 100\,\text{mM}$.

dimenionless rate constants for the fuel and oxidant reactions set to $\hat{K}_{F,O} = \hat{K}_{O,R} = 1$ and $\hat{K}_{F,R} = \hat{K}_{O,O} = 1 \times 10^{-6}$. This yields balanced fuel oxidation and oxidant reduction kinetics. It is apparent from Fig. 2 that for balanced kinetics the overall cell performance is identical for alkaline and acidic fuel cells while the electrode polarizations (overpotential-current traces) are not. The overpotentials are calculated by taking the difference between the electrode potential and the potential in the electrolyte just outside the diffuse region of the EDL. Overpotentials can be used as an indication of the magnitude of the electrostatic contribution to the rate of the electrode current. The electrostatic contribution is the portion of the electrode kinetic rate that is controlled by the potential difference across the Stern layer (i.e. the exponential terms in Eqs. (4) and (5)). The anode and cathode overpotential along with the voltage drop across the bulk electrolyte (ohmic losses) comprise the overall cell potential. The interdependency of cell potential, electrode current, and overpotentials for acidic and alkaline fuel cells is summarized in Table 2.

At high cell potentials or very low cell current density, the cathode overpotential decreases quite rapidly in an acidic fuel cell with increasing current density as shown in Fig. 2a. This rapid change in cathode overpotential near open circuit is known as the activation loss and is also reflected in the overall cell potential. The term "activation loss" comes from the idea that the cathode requires a larger deviation from the open circuit overpotential for the kinetics to be "activated". It is generally accepted that in low temperature fuel cells activation losses are the most important source of irreversability and occur mainly at the cathode in acidic fuel cells [1]. Fig. 2b shows that in an alkaline cell the anode suffers the activation loss while the cathode does not. Therefore, it is clear that the activation losses are present at the electrode where the working ion is consumed (i.e. cations at the cathode in acidic media and anions at the anode in alkaline media). The diminished activation losses in alkaline fuel cell cathodes is a well-known, observed result [1].

For mid to low current densities in an acidic fuel cell (Fig. 2a) the cathode overpotential is small which indicates that the net current at the cathode is not being significantly limited by the electrostatic portion of the reaction rate. This is not the case for the anode where the overpotential indicates that the net current is being retarded. The opposite occurs in an alkaline fuel cell, as shown in Fig. 2b. It would often be interpreted from Fig. 2a that the cathode, or from Fig. 2b that the anode, is the limiting electrode. However, this is not true for the devices presented as both electrodes were given equivalent kinetics. The difference in anode and cathode overpotential behavior is a direct consequence of the EDL and ionic transport effects on electrode kinetics, as discussed later.

3.2. Cell performance with unbalanced kinetics/reactants

To develop further differences between acidic and alkaline fuel cells, the device performance in response to unbalanced rate constants or reactant supply was studied. A VI plot and electrode polarizations for both media are presented in Fig. 3 for devices with reduced fuel reaction rate constants ($\hat{K}_{F,O} = 0.1$ and $\hat{K}_{F,R} = 1 \times 10^{-7}$). This creates a fuel cell that is kinetically limited at the anode. It can be seen that the overall cell performance of the acidic cell was significantly reduced from the balanced case while the alkaline cell was not. Interestingly, the cathode overpotential still shows strong signs of activation losses in the acidic fuel cell despite the anode kinetics being limited.

The VI plot and electrode polarizations are shown in Fig. 4 for acidic and alkaline fuel cells where the nominal concentration of fuel at the inlet was reduced to, $C_F^{Bulk} = 10\,\text{mM}$, while the other concentrations were unaltered. This creates a device that has strong reactant transport limitations at the anode. Again we see the performance of the acidic fuel cell is significantly decreased and the electrode overpotentials show similar behavior to that of the kinetically limited anode in Fig. 3. The alkaline fuel cell in Fig. 4 also shows a noticeable decrease in overall performance, although not

Table 2
Interdependency between salient metrics related to electrode kinetics.

	Electrode	η	$\lvert J_{,Net}\rvert$	$\lvert J_{,O}\rvert$	$\lvert J_{,R}\rvert$	Ψ_{Cell}	C_{C+}	C_{A-}	$\Delta\phi_S$	$\rho_e\lvert_{\text{Diffuse layer}}$
Acidic	Anode	↑	↑	↑	↓	↓	↓	N/A	↑	↓
	Cathode	↓	↑	↓	↑	↓	↑	N/A	↓	↑
Alkaline	Anode	↑	↑	↑	↓	↓	N/A	↑	↑	↓
	Cathode	↓	↑	↓	↑	↓	N/A	↓	↓	↑

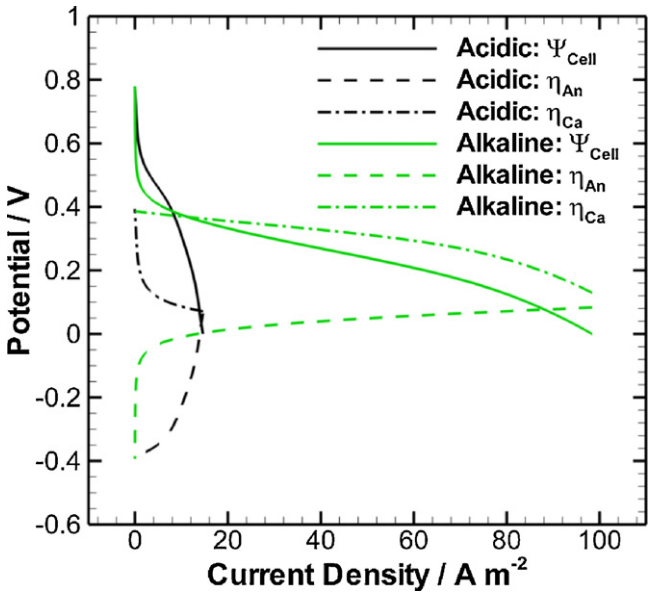

Fig. 3. Overall VI and electrode polarizations for both acidic and alkaline electrolytes in a LFFC with limited kinetics at the anode. The fuel reaction rate constants are reduced by a factor of ten, $\hat{K}_{F,O} = 0.1$ and $\hat{K}_{F,O} = 1 \times 10^{-7}$, while other rate constants remain unaltered.

as severe as the acidic fuel cell. The affect of the transport limitation is easily seen in the cell potential which rapidly decreases as cell current density approaches short circuit. Not surprisingly, this is reflected in the anode overpotential for alkaline fuel cell, which is being affected by a lack of fuel. In contrast, the transport limitations are difficult to discern in the acidic fuel cell because of the severely reduced performance.

To study how overall cell performance is affected with changing kinetics, the overall cell current density and the concentration of the working ion at the reaction plane of its consumption were obtained. Fig. 5 shows the electrode average concentration and current density as a function of the (a) fuel oxidation rate and (b) oxidant reduction rate. In Fig. 5a the fuel oxidation rate constant

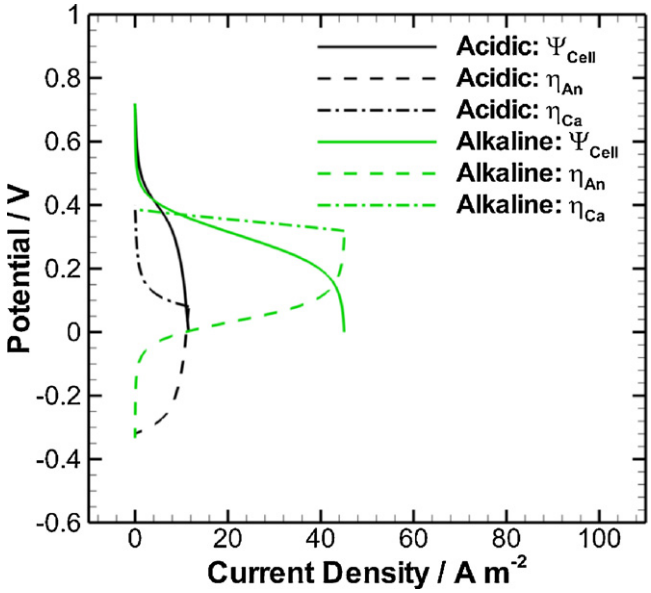

Fig. 4. Overall VI and electrode polarizations for both acidic and alkaline electrolytes in a LFFC with a reactant transport limitation at the anode. The nominal bulk concentration of fuel is reduced by a factor of ten, $C_F^{Bulk} = 10\,\text{mM}$, while other bulk concentrations remain unaltered.

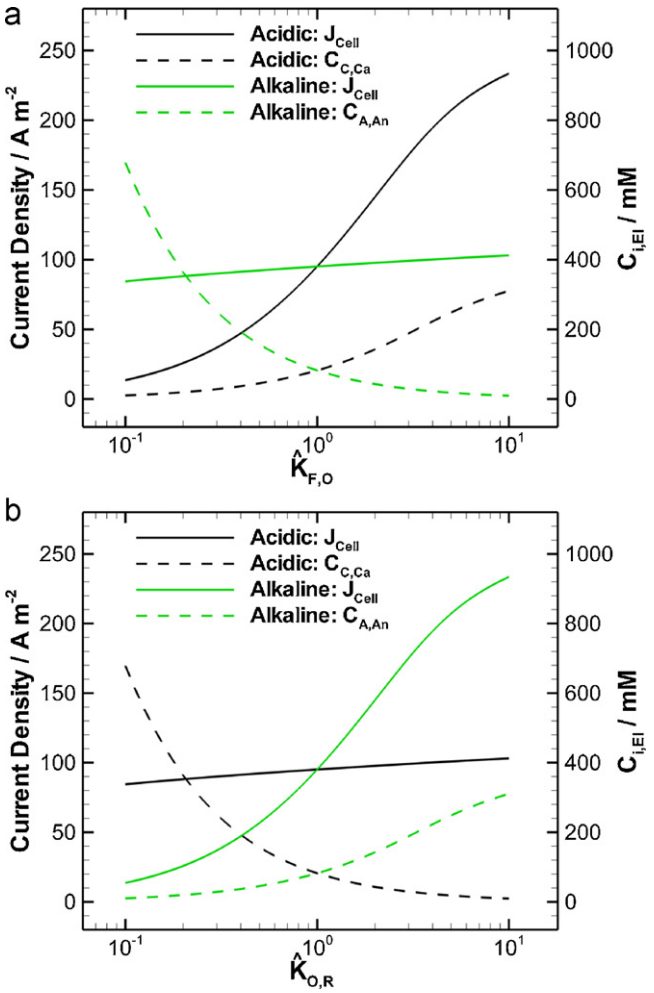

Fig. 5. Cell performance response in terms of cell current density to changing (a) fuel oxidation rate constant and (b) oxidant reduction rate constant for both the acidic and alkaline fuel cell. Also presented is the averaged concentration of the working ion at the electrode–electrolyte interface of its consumption (i.e. cations at the cathode and anions at the anode). The remaining rate constants were specified as: (a) $\hat{K}_{O,R} = 1$, $\hat{K}_{F,R} = \hat{K}_{O,O} = 1 \times 10^{-6}$, and (b) $\hat{K}_{F,O} = 1$, $\hat{K}_{F,R} = \hat{K}_{O,O} = 1 \times 10^{-6}$.

is swept from $\hat{K}_{F,O} = 0.1$ to $\hat{K}_{F,O} = 10$ while all other rate constants were unaltered and the cell potential maintained at $\psi_{Cell} = 100\,\text{mV}$. The cell current density of the acidic fuel cell shows a strong sensitivity to the fuel oxidation rate constant. The cell current density is initally very low at low rate constants and is high at higher rate constants. Where as the alkaline fuel cell current density shows a much less dramatic sensitivity to the changing rate constant. For changing oxidant reduction kinetics the results show a similar but opposite trend; the performance of an alkaline fuel cell is strongly affected while an acidic fuel cell is not. Fig. 5b shows the overall cell current density and working ion concentrations as the oxidant reduction rate constant is swept from $\hat{K}_{O,R} = 0.1$ to $\hat{K}_{O,R} = 10$. The cause of the different responses to improved kinetics is related to the diffuse region of the EDL. Whether or not the diffuse region hurts or helps depends on the concentration of the working ion at the reaction plane of its consumption.

For instance, in acidic media, the oxidant reduction has a concentration dependency (Eq. (4b)) on the working ion (cation). At low fuel oxidation kinetics the concentration of the cation at the cathode is severly reduced from the bulk value (Fig. 5a). As the rate constant increases the cation concentration at the cathode also significantly increases. Thus the acidic fuel cell gets the benefit of increasing fuel oxidation kinetics at the anode as well as increased

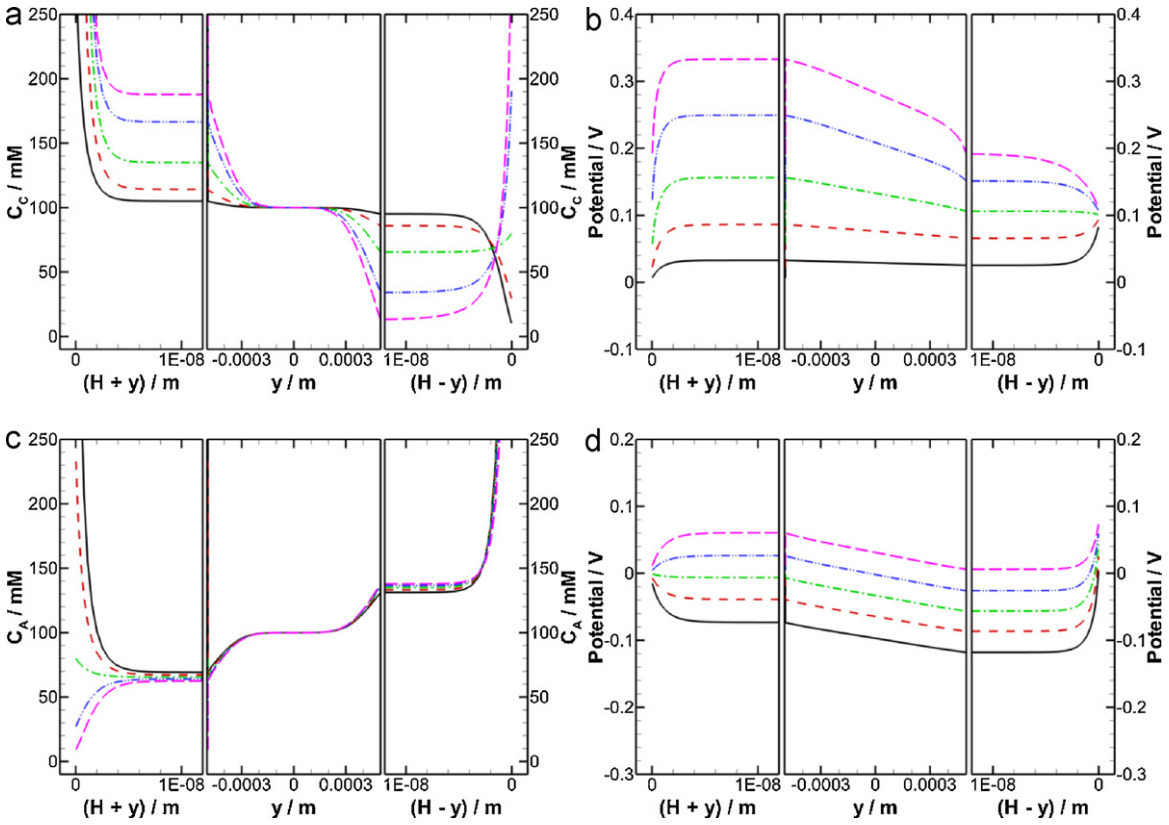

Fig. 6. Cross channel electrolyte potential and ion distributions for different fuel oxidation rate constants at $x = L/2$ ($\hat{K}_{F,O} = 0.10$: ▬, $\hat{K}_{F,O} = 0.32$: ▬ ▬ ▬, $\hat{K}_{F,O} = 1.00$: ▬ ▪ ▬, $\hat{K}_{F,O} = 3.16$: ▬ ▪ ▪ ▬, $\hat{K}_{F,O} = 10.0$: ▬ ▬). For an acidic fuel cell the (a) cation and (b) electrolyte potential distribution are presented and for an alkaline fuel cell the (c) anion and (d) electrolyte potential distribution are also presented. The distributions are only shown between the anode and cathode reaction planes. In other words, the distributions in the Stern layers are not shown. However, the potential change across the Stern layer can be determined by $\Delta\phi_S = \psi_{El} - \phi_{RP}$ where $\psi_{An} = 0$ V and $\psi_{Ca} = 0.1$ V for the results presented. The remaining rate constants were specified to $\hat{K}_{O,R} = 1$ and $\hat{K}_{F,R} = \hat{K}_{O,O} = 1 \times 10^{-6}$.

oxidant reduction kinetics at the cathode because of the increasing cation concentration. In alkaline media, however, at low fuel oxidation rates the concentration of the anion at the anode is above the bulk electrolyte concentration. This gives increased kinetics at the anode due to the anion concentration dependency (Eq. (5a)) despite the reduced fuel oxidation rate. As the rate constant increases the concentration of the anion at the anode decreases and is near zero at the larger rate constants. This limits the anode current density despite the increased fuel oxidation rate constant.

A result of the difference in performance response of acidic and alkaline fuel cells to changing anode kinetics is that for cases where the anode is the limiting electrode (low fuel oxidation rate constant), an alkaline fuel cell will outperform an acidic fuel cell. An important but not well understood phenomenon is that alcohol oxidation at the anode is better in an alkaline fuel cell than in an acidic fuel cell. If one assumes that alcohol oxidation is an inherently slow reaction, then the anode will be the limiting electrode. It can then be concluded that an acidic fuel cell will be more severely limited by these poor kinetics than an alkaline fuel cell. Therefore, the results in Fig. 5a offer an explanation for the superior alcohol oxidation performance in an alkaline fuel cell.

3.3. Electrolyte–electrode interface response to changing kinetics

The importance of ion transport is very apparent in Fig. 5 and is strongly influenced by the kinetic conditions at either electrode. To further investigate this, the electrolyte potential and working ion distribution across the channel at $x = L/2$ for different fuel oxidation rate constants are presented in Fig. 6 with $\psi_{An} = 0$ V and $\psi_{Ca} = 0.1$ V. The reults are presented in 3 domains; the anode diffuse region (left pannel), the bulk electrolyte (center pannel), and the cathode diffuse region (right pannel). The distribution of cations is presented in Fig. 6a for an acidic fuel cell. For low fuel oxidation rate constants there is a depletion of cations in the diffuse region at the cathode resulting in a negative charge density in that region. This corresponds to a positive Stern layer potential change as evidenced by the potential at the cathode reaction plane being less than the cathode electrode potential in Fig. 6b. As the fuel oxidation kinetics are increased, the potential change across the Stern layer ($\Delta\phi_S$) at the anode becomes more negative to retard the anodic current and maintain current conservation. Similarly, for higher fuel oxidation rate constants, the potential change across the cathodic Stern layer must also become negative to motivate the cathode. As the potential change across the cathodic Stern layer decreases to negative, the charge in the cathode diffuse region inverts from negative to positive (Fig. 6a). A consequence of the change in charge density (from negative to positive) in the cathode diffuse region is that the cations go from being depleted to a concentration greater than in the bulk electrolyte. The interdependency between ion concentration, the Stern potential change, and charge density in the diffuse region is summarized in Table 2.

The distribution of anions is presented in Fig. 6c for an alkaline fuel cell. In this case, for low fuel oxidation rate constants there is an excess of anions at the anode. Here, as the fuel oxidation kinetics are increased the potential change across the Stern layer ($\Delta\phi_S$) must become negative at the anode and less positive at the cathode to maintain current conservation (Fig. 6d). In the alkaline case the charge inversion occurs at the anode yielding a depletion of anions at the anode for large fuel oxidation rate constants. The differences in cell performance for reduced rate constants shown in

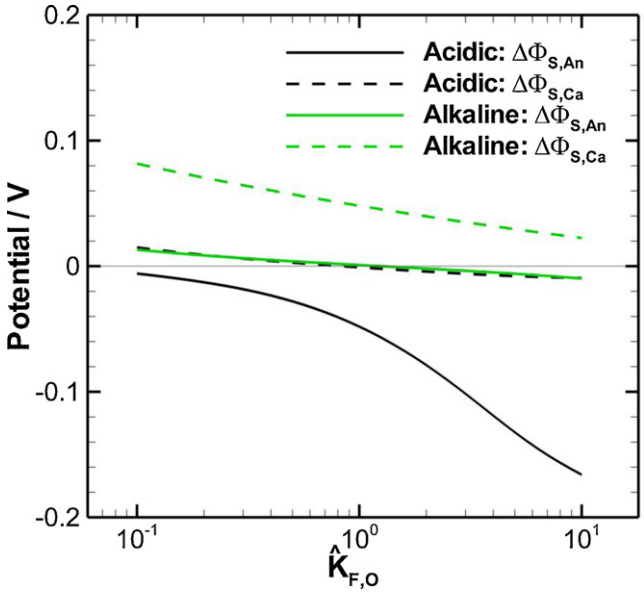

Fig. 7. The response of the potential changes across the Stern layer at both the anode and cathode for both the acidic and alkaline electrolyte for changing fuel oxidation rate constant. The values presented are the averages of the potential change distribution along the electrode. The remaining rate constants were specified to $\hat{K}_{O,R} = 1$ and $\hat{K}_{F,R} = \hat{K}_{O,O} = 1 \times 10^{-6}$.

Fig. 3 can be explained by the behavior of the working ion and electrolyte potential distributions in the diffuse regions presented here. We also studied the effect of changing reactant concentration on these distributions (not shown) to further understand the cell performance results presented in Fig. 4. It was found that the response of the diffuse region distributions and the overall cell current density for changing fuel concentration are very similar in qualitative trends to the results presented for changing fuel oxidation rate constants (Figs. 5 and 6). It can then be concluded that the role of the EDL in kinetic or transport limitations is comparable. For both the acidic and alkaline media it is evident that charge inversion and the potential difference across the Stern layer play a significant role in the overall cell response to changing kinetics. The average potential change across the Stern layer at both the anode and cathode for both media are presented in Fig. 7 as a function of the fuel oxidation rate constant. The charge inversion due to increasing fuel oxidation kinetics is reflected in the Stern layer potential change at the cathode in an acidic fuel cell and at the anode in an alkaline fuel cell. At slow fuel oxidation kinetics these Stern layer potential changes are positive and becomes negative at faster kinetics crossing through zero near $\hat{K}_{F,O} = 1$, which corresponds to balanced kinetics. The magnitude of the change across the Stern layer at the cathode for the alkaline fuel cell decreases with an increased fuel oxidation rate constant while the magnitude of the change at the anode for an acidic fuel increases drastically.

4. Conclusions

Acidic and alkaline fuel cells were studied numerically for a LFFC. The numerical model is based on the gFBV and PNP equations, and it is able to fully resolve the 2-dimensional diffuse region at the electrode–electrolyte interface. The overall cell performance and electrode polarizations were analyzed along with the cross channel ion and potential distributions. The results predicted cell behavior based on electrolyte composition that strongly correlates with known results from experiment. This work provides insight into the fundamental cause of these well known results and helps establish a clearer understanding of the electrolyte's interaction in electrode kinetics.

For balanced kinetics, it was shown that the magnitude of the cathode overpotential is lower than the magnitude of the anode overpotential in the power producing range for an acidic fuel cell. Thus, the cathode would be interpreted as the performance limiting electrode. However, in an alkaline fuel cell the cathode performance is enhanced and no longer appears to be the limiting electrode. Also, strong activation losses at the cathode are demonstrated in an acidic fuel cell which are eliminated in an alkaline fuel cell. It was then demonstrated that the improved cathode kinetics and reduced activation losses in an alkaline cells are a direct result of ion transport in the diffuse region of the EDL.

When unbalanced kinetics are considered in the anode side, the response in cell performance is different for acidic and anlkaline electrolytes. The trends for changing cathode kinetics are exactly opposite (e.g. alkaline fuel cells are sensative to changes in cathode kinetics while acidic fuel cells are not) of the trends shown for changing anode kinetics. It was found that while both cells benefit from improved kinetics at either electrode the effect of the EDL either multiplies or dampens this benefit. Considering this, we were able to determine that acidic fuel cells are more sensative to changes in anode kinetics than alkaline fuel cells. Therefore, for cases where the anode is the limiting electrode (low fuel oxidation rate constant) alkaline fuel cells perform better than acidic fuel cells. This provides an explanation for the superior alcohol oxidation performance in an alkaline fuel cell based on EDL effects.

Appendix A. Nomenclature

English characters

C	concentration, mM
C_s	Stern layer capacitance, F
D	diffusion coefficient, $m^2\ s^{-1}$
e^-	Electron
F	Faraday's constant, $C\ mol^{-1}$
H	half channel height, m
J	current density, $A\ m^{-2}$
$\hat{J}$	dimensionless current density
K	rate constant
$\hat{K}$	dimensionless rate constant
L	channel length, m
n	number of electrons involved in reaction
N	ionic flux, $mol\ s^{-1}\ m^{-2}$
P	pressure, Pa
R	ideal gas constant, $J\ K^{-1}\ mol^{-1}$
S	stoichiometric coefficient
T	absolute temperature, K
$\vec{V}$	fluid velocity vector, $m\ s^{-1}$
x	position along channel, m
y	position across channel, m
z	ionic charge

Greek characters

a	ratio of waste to electrolyte in bulk fluid
β	kinetics symmetry Factor
ε	permittivity, $F\ m^{-1}$
μ	viscosity, Pa s
ρ	density, $kg\ m^{-2}$
ρ_e	charge density, $C\ m^{-2}$
Φ	electrolyte potential, V
Ψ	electrode potential, V
ω	ion mobility, $m^2\ mol\ J^{-1}\ s^{-1}$

Subscripts

A^-	anion
An	anode
C^+	cation
Ca	cathode
Cell	device level values
E	electrolyte
El	electrode
F	fuel
O	oxidant
,O	oxidation
,R	reduction
RP	reaction plane
S	Stern layer
W	waste

References

[1] J. Larminie, A. Dicks, Fuel Cell Systems Explained, 2nd ed., John Wiley & Sons Ltd., West Sussex, UK, 2003.
[2] G.F. McLean, T. Niet, S. Prince-Richard, N. Djilali, Int. J. Hydrogen Energy 27 (2002) 507.
[3] C.Y. Wang, Chem. Rev. 104 (2004) 4727.
[4] A.Z. Weber, J. Newman, Chem. Rev. 104 (2004) 4679.
[5] J. Wu, X.Z. Yuan, H. Wang, M. Blanco, J.J. Martin, J. Zhang, Int. J. Hydrogen Energy 33 (2008) 1735.
[6] J. Wu, X.Z. Yuan, H. Wang, M. Blanco, J.J. Martin, J. Zhang, Int. J. Hydrogen Energy 33 (2008) 1747.
[7] M. Duerr, S. Gair, A. Cruden, J. McDonald, J. Power Sources 171 (2007) 1023.
[8] I. Verhaert, M. De Paepe, G. Mulder, J. Power Sources 193 (2009) 233.
[9] P. Björnbom, S.C. Yang, Electrochim. Acta 38 (1993) 2599.
[10] S.C. Yang, P. Björnbom, Electrochim. Acta 37 (1992) 1831.
[11] H. Weydahl, A.M. Svensson, S. Sunde, J. Electrochem. Soc. 156 (2009) A225.
[12] S. Mohan, S.O. Bade Shrestha, J. Fuel Cell Sci. Technol. 7 (2010) 041016.
[13] A. Verma, S. Basu, J. Power Sources 168 (2007) 200.
[14] M.Z. Bazant, K.T. Chu, B.J. Bayly, SIAM J. Appl. Math. 65 (2005) 1463.
[15] M. Van Soestbergen, Electrochim. Acta 55 (2010) 1848.
[16] P.M. Biesheuvel, M. Van Soestbergen, M.Z. Bazant, Electrochim. Acta 54 (2009) 4857.
[17] A.A. Franco, P. Schott, C. Jallut, B. Maschke, Fuel Cells 7 (2007) 99.
[18] P.M. Bieshuevel, A.A. Franco, M.Z. Bazant, J. Electrochem. Soc. 156 (2009) B225.
[19] I.B. Sprague, D. Byun, P. Dutta, Electrochim. Acta 55 (2010) 8579.
[20] I.B. Sprague, P. Dutta, Numer. Heat Transf. 59 (2011) 1.
[21] J.S. Spendelow, A. Wieckowski, Phys. Chem. Chem. Phys. 9 (2007) 2654.
[22] J.S. Spendelow, G.Q. Lu, P.J.A. Kenis, A. Wieckowski, J. Electroanal. Chem. 568 (2004) 215.
[23] J.L. Cohen, D.J. Volpe, H.D. Abruna, Phys. Chem. Chem. Phys. 9 (2007) 49.
[24] A.V. Tripkovic, K.D. Popovic, B.N. Grgur, B. Blizanac, P.N. Ross, N.M. Markovic, Electrochim. Acta 47 (2002) 3707.
[25] E.R. Choban, L.J. Markoski, A. Wieckowski, P.J.A. Kenis, J. Power Sources 128 (2004) 54.
[26] K.S. Salloum, J.D. Posner, J. Power Sources 195 (2010) 6941.
[27] I.B. Sprague, P. Dutta, S. Ha, J. Power Energy 223 (2009) 799.
[28] R.S. Jayashree, D. Egas, J.S. Spendelow, D. Natarajan, L.J. Markoski, P.J.A. Kenis, Electrochem. Solid-State Lett. 9 (2006) A252.
[29] E.R. Choban, J.S. Spendelow, L. Gancs, A. Wieckowski, P.J.A. Kenis, Electrochim. Acta 50 (2005) 5390.
[30] A. Bonnefont, F. Argoul, M.Z. Bazant, J. Electroanal. Chem. 500 (2001) 52.
[31] F. Chen, M.H. Chang, M.K. Lin, Electrochim. Acta 52 (2007) 2506.
[32] M.H. Chang, F. Chen, N.S. Fang, J. Power Sources 159 (2006) 810.
[33] A. Bazylak, D. Sinton, N. Djilali, J. Power Sources 143 (2005) 57.
[34] R.S. Jayashree, S.K. Yoon, F.R. Brushett, P.O. Lopez-Montesinos, D. Natarajan, L.J. Markoski, P.J.A. Kenis, J. Power Sources 195 (2010) 3569.
[35] J.O. Bockris, A.K.N. Reddy, M. Gamboa-Aldeco, Modern Electrochemistry 2A: Fundamentals of Electrodics, 2nd ed., Kluwer Academic/Plenum Publishers, New York, NY, 2000.